



DEGREE PROJECT IN TECHNOLOGY,
SECOND CYCLE, 30 CREDITS
STOCKHOLM, SWEDEN 2022

Gravity and surface tension-driven waves

KTH Master Thesis Report

Albin Hedblom

Author

Albin Hedblom ahedblom@kth.se
Mechanical Engineering
KTH Royal Institute of Technology

Place for Project

Fluid Physics Laboratory
KTH Department of Engineering Mechanics
Stockholm, Sweden

Examiner

Jens Fransson
KTH Royal Institute of Technology
Stockholm, Sweden

Supervisor

Jens Fransson
KTH Royal Institute of Technology
Stockholm, Sweden

Abstract

In this thesis, gravity and surface tension-driven water waves are investigated by designing an experimental setup to track wave patterns using a 300 fps high speed camera. This is done to reproduce the theoretical diagram of the dispersion relation for surface waves in different teaching contexts. Surface waves are dispersive, i.e. the phase speed depends on the wavelength.

Initially, the background theory for surface waves is presented and the differences between gravity and surface tension-driven waves are described. The conditions for deep and shallow water are also studied. Thereafter, a literature study is conducted to study similar experiments. Test experiments are then carried out where both direct and indirect methods of observing the waves are examined to determine which method generates the best images.

The water waves in the experiment are generated by dropping a 1.6 cm marble and a 4 mm water droplet into a 35 cm diameter hexagonal tank filled with 1–10 cm deep water. The waves are recorded from above and illuminated by backlighting with a 10 W LED panel. The experimental results show that a 1.6 cm marble generates wavelengths in the 0.4–3.5 cm range. Moreover, for a 4 mm water droplet, wavelengths in the range of 0.4–2.5 cm are generated.

Keywords

Gravity surface waves, capillary-gravity surface waves, dispersion, experiment

Sammanfattning

I den här uppsatsen undersöks gravitations- och ytspänningsdrivna vattenvågor genom att designa en experimentuppställning för att följa vågmönster med en 300 fps höghastighetskamera. Detta görs för att kunna reproducera det teoretiska diagrammet för dispersionsrelationen för ytvågor i undervisningssammanhang. Ytvågor är dispersiva, d.v.s. dess fashastighet beror på våglängden.

I rapporten presenteras inledningsvis bakgrundsteorin för ytvågor och skillnaderna mellan gravitations- och ytspänningsdrivna vågor beskrivs. Även förutsättningarna för djupt och grunt vatten studeras. Därefter genomförs en litteraturstudie för att studera liknande experiment. Sedan genomförs testexperiment där både direkta och indirekta metoder att observera vågorna undersöks för att avgöra vilken metod som genererar bäst bilder.

Vattenvågorna i experimentet genereras genom att släppa en 1.6 cm spelkula samt en 4 mm vattendroppe i en 35 cm diameter hexagonal tank, fyllt med 1–10 cm djupt vatten. Vågorna filmas från ovan samt belyses med motljus av en 10 W LED-panel. De experimentella resultaten visar att en 1.6 cm spelkula genererar våglängder i intervallet 0.4–3.5 cm. För en 4 mm vattendroppe genereras istället våglängder i intervallet 0.4–2.5 cm.

Nyckelord

Gravitationsdrivna ytvågor, ytspänningsdrivna ytvågor, dispersion, experiment.

Acknowledgements

I would like to express my deepest appreciation towards the people in the engineering mechanics department at KTH. I would like to direct a special thanks to my supervisor, Jens Fransson, for sharing his knowledge in the field of fluid mechanics and for his guidance which made this project possible. Furthermore, I would like to extend my most sincere gratitude towards Patricia Sujar Garrido, Francisco Jesus Lozano Vazquez, and Ramis Örlü for their knowledgeable input and support in enabling this project. Moreover, I would also like to extend my greatest appreciation to Santhosh Babu Mamidala and André Weingärtner for their practical help with the equipment in the Fluid Physics Laboratory.

Finally, I would like to direct an out of this world-thanks to my family. To my parents, Hillevi and Mats Hedblom, as well as my partner Elin Sundberg and my son Joel Hedblom. Without your support, this would not have been possible.

Stockholm, July 2022

Albin Hedblom

Nomenclature

η	Surface displacement [m]
λ	Wavelength [m]
μ	Dynamic viscosity [Pa·s]
ν	Kinematic viscosity [m^2/s]
ϕ	Velocity potential [1/s]
σ	Surface tension [Pa]
a	Amplitude [m]
c	Phase speed [m/s]
c_g	Group speed [m/s]
H	Water depth to undisturbed surface [m]
k	Wavenumber [rad/m]
p	Pressure [Pa]

Contents

1	Introduction	1
1.1	Background	1
1.2	Purpose	1
1.3	Scope	2
1.4	Delimitations	2
2	Theoretical background	3
2.1	Derivation of the governing equations for surface gravity waves . .	3
2.2	Boundary conditions	5
2.3	Dispersion relation for gravity waves	6
2.4	Dispersion relation for capillary-gravity waves	6
2.4.1	Limiting cases	8
2.5	Group speed	8
2.6	Classification of deep- and shallow water waves.	9
2.6.1	Deep-water approximation	9
2.6.2	Shallow-water approximation	11
2.7	Perturbation pressure	12
3	Literature review	14
3.1	Similar experiments	14
3.2	Flow visualisation techniques	16
3.2.1	Illumination techniques	16
3.2.2	Image processing	16
4	Designing the experiment	18
4.1	Test Experiments	18
4.1.1	Direct methods	18
4.1.2	Indirect methods	20
4.1.3	High speed camera	21
4.1.4	Water depth	22
4.1.5	Avoiding problems from reflections	22
4.1.6	Problems due to splashes	23
4.2	Experimental setup	23
4.3	Image processing procedure	25
4.4	Measuring the wave speed	26

CONTENTS

4.4.1	Wave tracking	28
5	Results	31
5.1	Results from the marble	31
5.2	Results from the droplet	37
6	Discussion	42
6.1	Sources of uncertainty	42
6.1.1	Water depth and noise	42
6.1.2	Errors due to illumination	42
6.1.3	Errors due to image processing	42
6.2	Short and long wavelengths	43
7	Conclusions	44
7.1	Future Work	45
	References	47

Chapter 1

Introduction

Most of us have probably thrown a rock into the water and observed the wave patterns formed on the surface. In the same way, most people have probably looked out the window on a rainy day and seen the ripples that form when raindrops fall into a puddle of water. These two phenomena are typical examples of water surface waves. You may remember how it looks like when these circular waves propagate, growing bigger and bigger as time goes on. Something that may not be as obvious is that the wave pattern formed from a thrown stone can look very different compared to the pattern formed from a falling water drop. This is because two different restoring forces dominate in the two cases. Gravity is the dominant restoring force when a rock causes a disturbance on the surface. In the case of a disturbance caused by a drop of water, the surface tension is the dominant restoring force. In addition, these surface waves are dispersive, i.e., the wave speed depends on the wavelength (Lighthill, 1978), with opposite behaviour when comparing the two restoring forces.

1.1 Background

This work aims to design, manufacture and carry out an experiment to reproduce the dispersion relation in Figure (2.4.2), which shows how the phase speed varies with wavelength. Wavelengths and wave speeds are to be measured for the textbook example "stone and drop in a pond". The experiment will be carried out for the two limiting cases, gravity surface waves (GSW) and capillary surface waves (CSW), in both shallow and deep water.

1.2 Purpose

The purpose of this experiment is to evoke interest in the field of fluid mechanics among students who are new to the subject. The experiment also intends to

CHAPTER 1. INTRODUCTION

convey intuition and understanding of how theory and practice connect in the subject of surface waves.

1.3 Scope

The scope of the thesis consists of

- Literature study on the theoretical background of the dispersion of water waves.
- Literature study on similar experiments.
- Create design suggestions for the experimental setup and evaluation of these.
- Construction of the experimental setup including water tank with adjustable depth and objects releasing mechanism.
- Image processing and analysis of data.

1.4 Delimitations

The scope of the experiment is limited to the treatment of linear capillary and gravity-driven interface waves on the free surface between air and water. Hence, the experiment is limited to not considering the chaotic initial state at the time of impact. Furthermore, the measurements can not be performed longer than until the leading wave hits and reflect at the wall.

Chapter 2

Theoretical background

In fluid mechanics, surface waves, or interface waves, can be seen as a traveling oscillating disturbance to the free surface between two media. An example close to mind is the water waves formed in the interface between water and air. The waves get sustained by an interplay between the fluid inertia and a restoring force. The restoring force tries to bring back the system to its undisturbed state, and the inertia causes the system to overshoot. For surface capillary-gravity waves (CGW), the restoring forces are gravity and surface tension (Kundu et al., 2016).

2.1 Derivation of the governing equations for surface gravity waves

The surface wave problem, such as in Figure (2.1.1), is in general non-linear. However, by assuming that the amplitude of the wave, a , is much smaller than

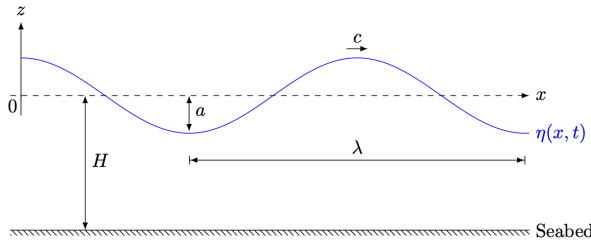


Figure 2.1.1: Properties of two-dimensional surface waves traveling over constant water depth, H . $\eta(x, t)$ is the vertical displacement of the free surface.

the wavelength, λ , together with the assumption that the amplitude is much

smaller than the undisturbed water depth, H ,

$$\begin{cases} a \ll \lambda \\ a \ll H \end{cases} \quad (2.1)$$

the equations can be linearized. Moreover, the wave frequency is assumed to be large in comparison to the Coriolis frequency, and hence, the earth's rotation can be neglected. At the moment, surface tension is neglected. By assuming that the viscosity of the fluid is negligible and that the wave motion is generated from rest, the motion can be considered to be irrotational according to Kelvin's circulation theorem, and hence the velocity potential can be used.

The equations of motion for an inviscid, incompressible fluid are the continuity equation (conservation of mass) and the Euler's equation (conservation of momentum) respectively

$$\nabla \cdot \vec{u} = 0 \quad (2.2)$$

$$\frac{\partial \vec{u}}{\partial t} + \vec{u} \cdot \nabla \vec{u} = -\frac{1}{\rho} \nabla p + \vec{g}. \quad (2.3)$$

Here, ρ is the density of the fluid, p is the pressure, \vec{g} is the gravitational acceleration vector, and \vec{u} is the velocity vector. The velocity vector is formulated as

$$\vec{u} = (u, v, w) \quad \text{2D} \Rightarrow \quad \vec{u} = (u, w), \quad (2.4)$$

where u and w are the horizontal and vertical velocity components, respectively. By introducing the velocity potential (ϕ)

$$\vec{u} \equiv \nabla \phi \quad (2.5)$$

and inserting this into the continuity equation, eq. (2.2), Laplace's equation (in 2D) is attained

$$\nabla^2 \phi = \frac{\partial^2 \phi}{\partial x^2} + \frac{\partial^2 \phi}{\partial z^2} = 0. \quad (2.6)$$

Euler's equation can be reformulated by using the vector identity (Råde, 2004),

$$\vec{u} \times (\nabla \times \vec{u}) = \nabla \left(\frac{1}{2} \vec{u} \cdot \vec{u} \right) - \vec{u} \cdot \nabla \vec{u} \quad (2.7)$$

and recalling that the motion is irrotational, that is

$$\nabla \times \vec{u} = \vec{0}. \quad (2.8)$$

Moreover, gravity is working only in the vertical z -direction

$$\vec{g} = \nabla(-gz). \quad (2.9)$$

By inserting these expressions into Euler's equation, the following expression is attained

$$\frac{\partial}{\partial t}(\nabla \phi) + \nabla \left(\frac{1}{2} \nabla \phi \cdot \nabla \phi \right) = -\frac{1}{\rho} \nabla p - \nabla(gz). \quad (2.10)$$

If ϕ is a smooth function, then ∇ can be moved out of the parentheses in the first term. An integration of this expression yields an arbitrary integration function that only depends on time. Since the function is arbitrary, it can conveniently be set to 0. This is possible since incorporating $G(t)$ in ϕ by the substitution

$$\phi \rightarrow \phi + \int_0^t G(s)ds \quad (2.11)$$

does not affect the velocity field. Doing this, the Bernoulli equation is acquired

$$\frac{\partial \phi}{\partial t} + \frac{1}{2} \nabla \phi \cdot \nabla \phi + \frac{1}{\rho} p + gz = 0. \quad (2.12)$$

2.2 Boundary conditions

There are three boundary conditions (BCs) to be satisfied.

- The dynamic boundary condition (DBC)
- The kinematic boundary condition (KBC)
- The bed boundary condition (bed BC)

The dynamic BC states that the pressure at the surface is equal to the ambient pressure since surface tension is neglected at the moment

$$\frac{\partial \phi}{\partial t} + \frac{1}{2} \nabla \phi \cdot \nabla \phi + g\eta = 0 \quad \text{at } z = \eta(x, t). \quad (2.13)$$

The kinematic BC states that a fluid particle on the surface, stays on the surface

$$w = \frac{D\eta}{Dt} \quad \text{at } z = \eta(x, t). \quad (2.14)$$

Here, $\frac{D}{Dt}$ is the material derivative, and w is the vertical velocity at the surface which can be written out as

$$\frac{\partial \phi}{\partial z} = \frac{\partial \eta}{\partial t} + \frac{\partial \phi}{\partial x} \frac{\partial \eta}{\partial x} \quad \text{at } z = \eta(x, t). \quad (2.15)$$

The bed BC is an impermeability condition; it says that the normal velocity must be zero at the bottom

$$w = \frac{\partial \phi}{\partial z} = 0 \quad \text{at } z = -H. \quad (2.16)$$

By linearizing, these BCs can be formulated as

$$\begin{cases} (\text{LDBC}) \quad \frac{\partial \phi}{\partial t} + g\eta = 0 & \text{at } z = 0 \\ (\text{LKBC}) \quad \frac{\partial \phi}{\partial z} = \frac{\partial \eta}{\partial t} & \text{at } z = 0 \\ (\text{Bed BC}) \quad \frac{\partial \phi}{\partial z} = 0 & \text{at } z = -H. \end{cases} \quad (2.17)$$

Here, the dynamic and kinematic BCs are evaluated at $z = 0$ instead of at $z = \eta$, this is a first-order Taylor approximation which holds for small amplitude waves.

2.3 Dispersion relation for gravity waves

Surface water waves show a dispersive behavior, meaning that waves with different wavelengths travel at different speeds. The phase speed of a propagating surface wave is defined as

$$c = c(\lambda) = \frac{\omega}{k}, \quad (2.18)$$

and gives the speed of the individual wave crests. To show that the wave system is dispersive, the surface displacement is assumed to be sinusoidal

$$\eta(x, t) = a \cos(kx - \omega t). \quad (2.19)$$

Here, a is the amplitude, $k = 2\pi/\lambda$ is the wavenumber, and ω is the angular frequency. By assuming that the solution to the gravity wave- (GW)-problem is of separable form

$$\phi(x, z, t) = f(z) \sin(kx - \omega t). \quad (2.20)$$

Applying this to the Laplace equation yields the differential equation

$$\frac{\partial^2 f}{\partial z^2} - k^2 f = 0. \quad (2.21)$$

Solving this equation, using the Bed BC to determine constants, the following solution is attained

$$\phi(x, z, t) = \frac{a\omega}{k} \frac{\cosh\{k(z + H)\}}{\sinh(kH)} \sin(kx - \omega t). \quad (2.22)$$

To determine the dispersion relation for GWs, the partial time derivative of LDBC is taken and combined with the LKBC

$$\frac{\partial}{\partial t}(\text{LDBC}) = \frac{\partial^2 \phi}{\partial t^2} + g \frac{\partial \phi}{\partial z} = 0 \quad \text{at } z = 0. \quad (2.23)$$

Finally, by combining equations (2.18),(2.22), and (2.23), the dispersion relation for GWs can be expressed as

$$c^2 = \frac{g}{k} \tanh(kH). \quad (2.24)$$

2.4 Dispersion relation for capillary-gravity waves

In contrast to gravity surface waves, capillary-gravity waves (CGW) are also affected by surface tension, σ . Presence of surface tension leads to a modified version of the LDBC in equation (2.17). From Figure (2.4.1) a force balance on the surface element ds can be written in the radial direction as

$$-P_{atm} ds + P_f ds + 2\sigma \sin\left(\frac{d\theta}{2}\right) = 0. \quad (2.25)$$

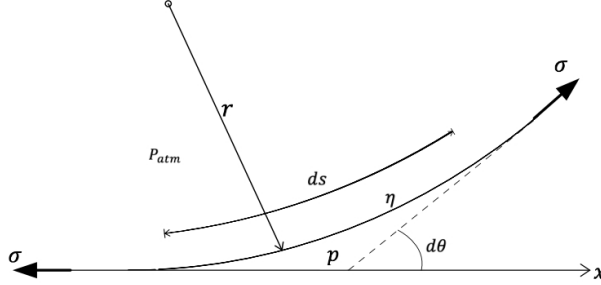


Figure 2.4.1: Forces acting on a small surface element on the free surface.

Which for small angles, $ds \approx rd\theta$ and $\sin(\frac{d\theta}{2}) \approx \frac{d\theta}{2}$, becomes

$$-P_{atm}rd\theta + P_f rd\theta + 2\sigma \frac{d\theta}{2} = 0 \quad \Rightarrow \quad P_f - P_{atm} = -\frac{\sigma}{r} . \quad (2.26)$$

Where $\frac{1}{r}$ is the curvature of the surface η and can be approximated as

$$\frac{1}{r} \approx \frac{\partial^2 \eta}{\partial x^2} . \quad (2.27)$$

This makes it possible to include the surface tension in the pressure term in Bernoulli's equation (2.12) as follows

$$\frac{\partial \phi}{\partial t} + g\eta - \frac{\sigma}{\rho} \frac{\partial^2 \eta}{\partial x^2} = 0 \quad \text{at } z = 0 . \quad (2.28)$$

This is the modified linear dynamic BC (mod. LDBC). In the same way as with GWs, the dispersion relation is derived by taking the time derivative of the mod. LDBC and combining the expression with LKBC in (2.17).

$$\frac{\partial}{\partial t} (\text{mod. LDBC}) = \frac{\partial^2 \phi}{\partial t^2} + g \frac{\partial \phi}{\partial z} + \frac{\sigma}{\rho} \frac{\partial^3 \phi}{\partial z^3} = 0 \quad \text{at } z = 0 . \quad (2.29)$$

And in the same way as in chapter 2.3, by combining equations (2.22) and (2.29), the dispersion relation for the CGW can be expressed as

$$c^2 = \left(\frac{g}{k} + \frac{k\sigma}{\rho} \right) \tanh(kH) . \quad (2.30)$$

By using eq. (2.18), the dispersion relation can be expressed in the alternative form

$$\omega^2 = \left(gk + \frac{\sigma k^3}{\rho} \right) \tanh(kH) . \quad (2.31)$$

2.4.1 Limiting cases

Looking at Eq. (2.30), there are two limiting cases. If

$$\frac{g}{k} \ll \frac{k\sigma}{\rho} \quad (2.32)$$

then surface tension is dominating, and gravity is negligible. From this expression, the capillary wavelength can be defined as

$$\lambda_{cap} \equiv \sqrt{\frac{\sigma}{\rho g}}. \quad (2.33)$$

Hence, if $\lambda >> \lambda_{cap}$, surface tension can be neglected instead. Looking at Figure (2.4.2) below it is apparent that there is a minimum wave speed, c_{min} , for a certain wavelength $\lambda = \lambda_{min}$. Figure (2.4.2) displays water at room temperature, $T = 20^\circ \text{C}$, for which the surface tension is $\sigma = 72.75 \cdot 10^{-3} \text{ N/m}$ and the density is $\rho = 998 \text{ kg/m}^3$, according to (Vargaftik et al., 1983) and (Cengel, 2015) respectively. Under these circumstances the corresponding λ where c_{min} takes place is found to be $\lambda_{min} = 1.71 \text{ cm}$ which yields a minimum wave speed, $c_{min} = 23.1 \text{ cm/s}$.

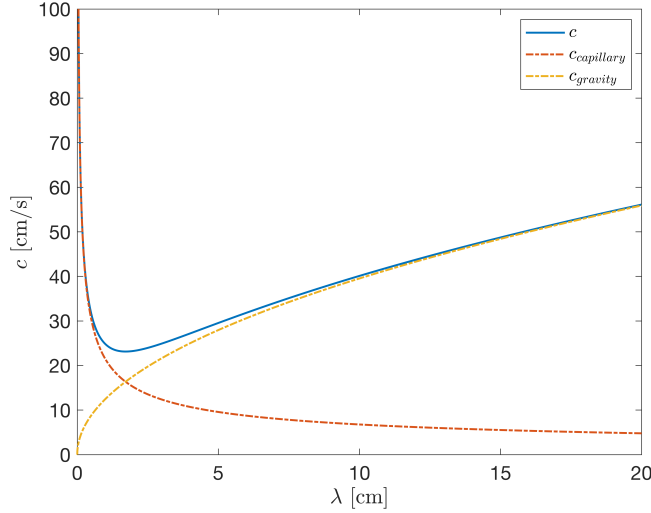


Figure 2.4.2: Dispersion relation for surface capillary-gravity wave. The dotted lines represent the limiting cases. The yellow dotted line is a pure gravity wave. The red dotted line is a pure capillary wave.

2.5 Group speed

As mentioned in section (2.3), in a dispersive system, individual wave components of different wavelengths travel at different speeds, causing waves

to disperse from each other. The individual wave components make up an envelope of waves, this is illustrated in Fig. (2.6.2). The envelope, and also the energy of the wave, travel with the group speed. The group speed is defined as

$$c_g = \frac{\partial \omega}{\partial k} . \quad (2.34)$$

By differentiating the alternative form for the dispersion relation in equation (2.31) an explicit expression for the group speed, c_g , is attained

$$c_g = \frac{c}{2} \left[\frac{1 + 3k^2 \lambda_{cap}^2}{1 + k^2 \lambda_{cap}^2} + \frac{2kH}{\sinh(2kH)} \right] . \quad (2.35)$$

2.6 Classification of deep- and shallow water waves.

To distinguish between what is meant by deep and shallow water, a classification is needed. Kundu et al., 2016 classifies water depth as shallow or deep if the approximations of the dispersion relation have an accuracy of $\leq 3\%$. Meaning that the simplified deep- and shallow-water approximations of eq. (2.30) are allowed to deviate no more than 3% from the unaltered equation to be accurate.

2.6.1 Deep-water approximation

The deep-water approximation is formulated as $kH \rightarrow \infty$. From Figure (2.6.1) it is apparent that this leads to $\tanh(kH) \rightarrow 1$. And hence, the dispersion relation in eq. (2.30) is approximated as

$$c = \sqrt{\frac{g}{k}} . \quad (2.36)$$

With a 3% accuracy of the phase speed, this approximation holds for $H > 0.28\lambda$. In table (2.6.1) the limiting case phase and group speeds are summarized.

Table 2.6.1: Summary of c (2.30) and c_g (2.35) for deep water approximation, $kH \rightarrow \infty$.

Limiting case	Phase speed, c	Group speed, c_g
Pure gravity wave $\lambda \gg \lambda_{cap}$ i.e. $\lambda_{cap} \rightarrow 0$	$c = \sqrt{\frac{g}{k}}$	$c_g = \frac{1}{2}c$
Pure capillary wave $\lambda \ll \lambda_{cap}$ i.e. $\lambda_{cap} \rightarrow \infty$	$c = \sqrt{\frac{k\sigma}{\rho}}$	$c_g = \frac{3}{2}c$

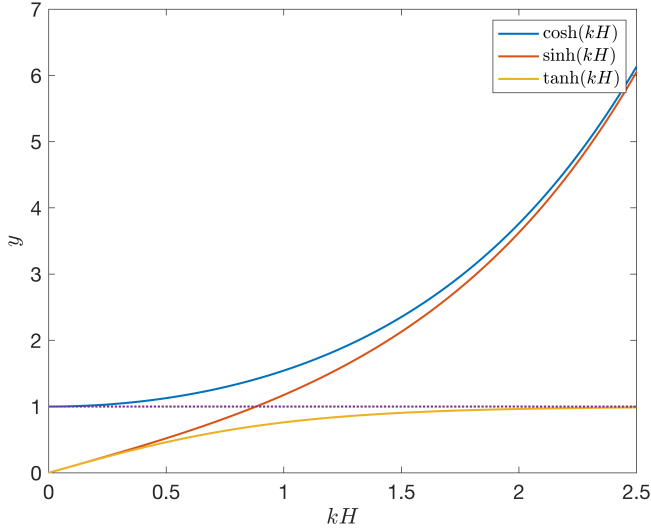


Figure 2.6.1: Plots of hyperbolic functions.

GWs in deep water are dispersive. Also, the phase speed is larger than the group speed for GWs, which means that individual wave crests travels faster than the wave groups (Acheson, 1990). Looking at Figure (2.6.2), which show the superposition of two sinusoidal waves with the same amplitude, a , but with slightly different wavenumber, $k_1 \neq k_2$, i.e.,

$$\begin{aligned} \eta &= a \cos(k_1 x - \omega_1 t) + a \cos(k_2 x - \omega_2 t) \\ &= 2a \cos\left(\frac{1}{2}\Delta kx - \frac{1}{2}\Delta\omega t\right) \cos(kx - \omega t) . \end{aligned} \quad (2.37)$$

For GWs, wave crests are born at the trailing edge and travels forward through the envelope and disappears at the leading edge.

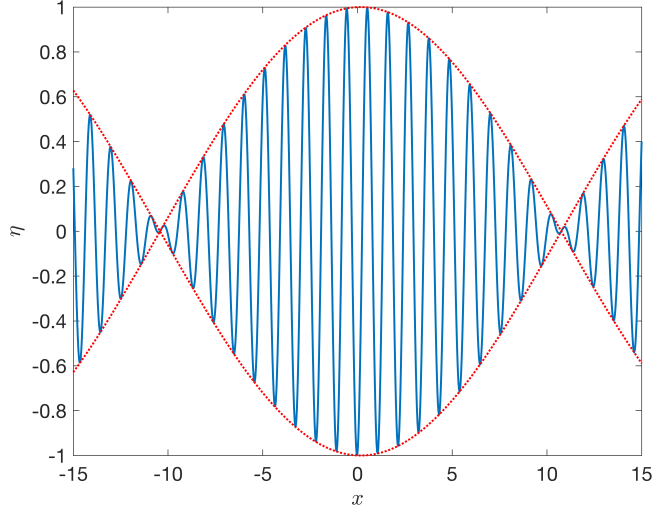


Figure 2.6.2: Illustration of individual waves forming a wave packet, the individual crests travel with the phase speed c , the entire envelope travels with the group speed c_g .

In contrast, for CW's, the phase speed is lower than the group speed. This means that individual crests are born at the leading edge and travel backwards through the envelope and disappear at the trailing edge.

2.6.2 Shallow-water approximation

The shallow-water approximation is formulated as $kH \rightarrow 0$. From Figure (2.6.1) it is apparent that this leads to $\tanh(kH) \rightarrow kH$. And hence, the dispersion relation in eq. (2.30) is approximated as

$$c = \sqrt{gH} . \quad (2.38)$$

From this, it is apparent that GWs are not dispersive in shallow water. This approximation holds for $H < 0.07\lambda$ with a 3% accuracy of the phase speed. In table (2.6.2) the limiting cases phase and group speeds are summarized.

Table 2.6.2: Summary of c (2.30) and c_g (2.35) for shallow water approximation, $kH \rightarrow 0$.

Limiting case	Phase speed, c	Group speed, c_g
Pure gravity wave $\lambda \gg \lambda_{cap}$ i.e. $\lambda_{cap} \rightarrow 0$	$c = \sqrt{gH}$	$c_g = c$
Pure capillary wave $\lambda \ll \lambda_{cap}$ i.e. $\lambda_{cap} \rightarrow \infty$	$c = k\sqrt{\frac{H\sigma}{\rho}}$	$c_g = 2c$

2.7 Perturbation pressure

By introducing the pressure perturbation as

$$p' \equiv p + \rho g z . \quad (2.39)$$

And applying this on the linearized version of Bernoulli's equation in eq. (2.12), the following is attained

$$p' = -\rho \frac{\partial \phi}{\partial t} . \quad (2.40)$$

By combining eq. (2.40) and the time derivative of the velocity potential, eq. (2.22), an explicit expression for the perturbation pressure is attained as

$$p' = \rho g a \frac{\cosh\{k(z+H)\}}{\cosh(kH)} \cos(kx - \omega t) . \quad (2.41)$$

For deep-water waves, $kH \rightarrow \infty$, the perturbation pressure in eq. (2.41) can be simplified to

$$p' = \rho g a e^{kz} \cos(kx - \omega t) . \quad (2.42)$$

Figure (2.7.1) shows the behavior of the the perturbation pressure for a deep-water wave, from this, it is clear that the pressure perturbation decreases exponentially with increasing water depth.

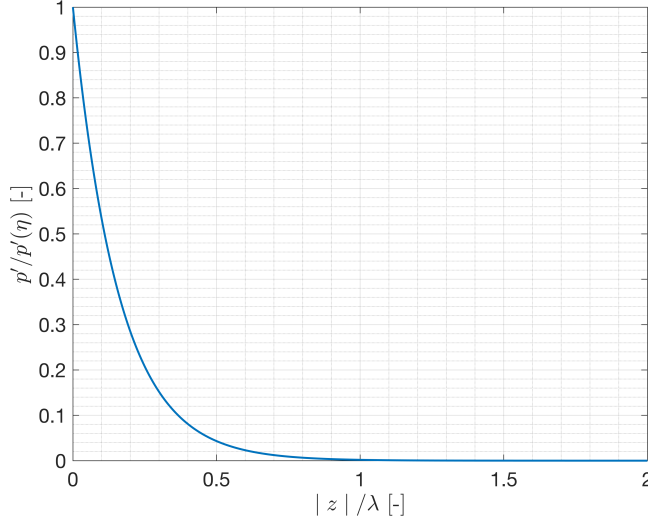


Figure 2.7.1: Behavior of pressure perturbation with increasing water depth. p' normalized by the perturbation pressure at the surface. Water depth normalized by the wavelength.

Already at a water depth of one wavelength, the perturbation pressure is about 0.2 % of the value at the surface. This makes the use of pressure gauges insufficient for this experiment.

In contrast, for shallow-water waves, $kH \rightarrow 0$, the perturbation pressure in eq. (2.41) can be simplified to

$$p' = \rho g a \cos(kx - \omega t). \quad (2.43)$$

From this, it is clear that the perturbation pressure in shallow water is independent of depth, i.e., the pressure is hydrostatic. Hence, a pressure gauge placed at the bottom could be sufficient for an experiment solely interested in shallow-water waves.

Therefore in the present study, optical measurement techniques will be used to track the waves developed in the different cases. As it will be shown in the literature review in Chapter (3).

Chapter 3

Literature review

In this chapter, similar experiments as planned in this work are reviewed. Moreover, sections 3.2–3.2.1 account for what the literature says about flow visualisation and illumination techniques.

The experiments covered in section 3.1 have looked at surface waves with several different measurement techniques. The measurement techniques used in the experiments include capacitance probe systems, ultrasonic probe systems, and optical measurement techniques using video cameras. The experiments have used different ways of generating surface waves, such as falling droplets, moving pistons, oscillating paddles, and a suction fan.

3.1 Similar experiments

In an experiment by Strickland et al., 2015, a spatiotemporal measurement of surfactant distribution on CGWs is conducted. A cylindrical tank with a diameter of 29.2 cm filled with a water depth of 0.37 cm is used for the experiment. The waves were generated by vertically oscillating the tank. The surface height was monitored by moiré imaging. The water surface is illuminated by a reference pattern and analyzed by ray tracing together with nonlinear fitting. The authors found that the surfactant accumulated at the leading edge of the traveling waves and in the throughs of the standing waves.

In the experiment by Craeye et al., 1999, a quadratic 1.1 x 1.1 m tank with a water depth of 20 cm was used to look at the height profiles of ring-waves. The waves were generated by a falling water droplet, produced by a hypodermic needle, and dropped from heights between 1 and 5.5 m above the surface, corresponding to 55%, 81%, and 91% of terminal velocity. The waves were observed indirectly by recording the effect on a mirrored image of a straight line on the surface with a 25 FPS video camera. The conclusion from this experiment was that the droplets produced waves with a characteristic

wavenumber of 0.2 mm^{-1} , which corresponds to a characteristic wavelength of 3.14 cm . Moreover, the authors also concluded that only about 1% of the kinetic energy is converted into ring-waves. The authors assume that the rest of the energy is transformed into vorticity, propagating vertically through the liquid. However, this is not part of the scope of the experiment and is not further elaborated upon. Another finding from the experiment is that the ring-wave energy strongly depends on the size of the droplet.

In the experiment by Zhang, 1995, a 2.4 m wide and 44 m long rectangular closed channel was used to look at CGWs and capillary waves (CW) generated by wind at a water depth of 1.2 m . The waves were generated by wind, driven by a suction fan at the end of the channel. To dissipate the waves, an absorber was placed at the end of the channel. To measure the waves, an optical method of placing a Fresnel lens deep below the surface is used. A 35 mm film camera records the refracted light from above the surface at a distance much larger than the camera's field of view (FOV). The experimental setup allows for a minimum of 3 mm wavelengths to be resolved. According to the authors, CWs are mainly found as parasitics on the downwind face of GWs. The parasitic CWs have a maximum wavelength of 1 cm .

Moreover, in the experiment by Taklo et al., 2015, a 0.5 m wide and 24.6 m long wave tank with a water depth of 0.5 m was used to measure the dispersion relation for random GSWs. The waves were generated by a hydraulic piston wave maker. To reduce reflections, a wave-absorbing beach was used at the end of the tank. To monitor the waves, 16 non-intrusive ultrasonic probes were placed 6, 12, and 15 cm above the mean water surface level. The authors found that the measured dispersion relation deviated from the linear theory above the spectral peak when the bandwidth was sufficiently narrow. The authors also found that, for a broad-banded spectrum, the measured dispersion relation shows good agreement with the linear theory. However, the authors do not elaborate on what they mean by good agreement.

Finally, in the experiment by Scott, 1981, a 95 mm wide and 1 m long rectangular channel was used to look at the propagation of CGWs on a clean water surface. CGWs in the frequency range of $2\text{--}10 \text{ Hz}$ were investigated at a water depth of 29 mm . A wave-absorbing beach was placed at the end of the channel to reduce reflections. The waves were generated by an electrodynamic vibrator and an oscillating Perspex paddle. The position of the wave surface was monitored by a TE200 Wayne-Kerr capacitance probe system. The author found that the experimental results show good agreement with the linearized hydrodynamic theory, with a mean deviation of 0.75% between measured and theoretical wavelengths. Another finding was that theoretical and measured wavelengths agreed better for longer-period waves than for shorter periods.

3.2 Flow visualisation techniques

Naturally visible phenomena are those that can be observed without having to introduce foreign objects or disturbances into the fluid. Surface waves are examples of naturally visible phenomena. Although surface waves are naturally visible, the visualization can be made more evident by introducing foreign objects into the fluid, such as fluorescent dyes or yarns, so-called marker techniques (Tavoularis, 2005). Flow visualization, such as an optical image, is generally a qualitative method. However, by using computers, the images can be processed, and quantitative data can be extracted and analyzed using image processing and analysis programs, e.g., MATLAB with its Image Processing Toolbox. To perform a visualization experiment, optical access to the fluid is needed, i.e., an open container and/or transparent walls. When collecting optical data through multiple mediums, such as air - transparent wall - water, refraction of light occurs due to the different refractive indices of the mediums (Tropea et al., 2007).

3.2.1 Illumination techniques

Illumination by regular thermal light sources is often used in a floodlight arrangement. However, the positioning of the light sources is still of importance. According to Tavoularis, 2005, the optimal way of recording a flow when using markers is to view it perpendicular to the direction of the flow and at the same time illuminate the test section at a 120° angle with either back- or front lighting. Collimators can be used to increase the intensity of the light and makes it possible to direct the light to reduce reflections.

A laser produces high-intensity illumination on a small area. To increase the illuminated area a laser-sheet technique can be used. This is done by shine the laser beam through a cylindrical lens, e.g., a glass rod, which creates a diverging laser sheet (Tavoularis, 2005).

In Sweden, the alternate current (AC) frequency used in the power sockets are 50 Hz, i.e., lamps powered by AC are powered in cycles of 50 times per second. This leads to a common illumination issue for high-speed cameras, which are flickering. There are multiple ways to eliminate the problem with flickering. One way to get rid of unwanted flickering is by using a continuous light source, e.g., a continuous laser. The flickering issue can also be eliminated by powering the lights with direct current (DC) instead of AC. Furthermore, flickerless illumination can be produced by backlighting high-intensity LED lights through a diffuser made of thin drafting paper (Zou et al., 2013).

3.2.2 Image processing

In the article by Ströbel, 2011, the author demonstrates dispersion of water waves by using a ripple tank. A high-power LED light projects the waves via a 45° inclined mirror to a vertical projection screen below the tank. The wave

CHAPTER 3. LITERATURE REVIEW

patterns are recorded at the projection screen with a 60 fps progressive mode camera. According to the author, the wave crests act as cylindrical collecting lenses, and can therefore be seen as bright lines on the projection screen. Furthermore, the author notes that there is a problem with the projection screen being unequally illuminated "To avoid this problem with the recorded wave patterns, a reference image without any waves excited is recorded before each series of waves."

Chapter 4

Designing the experiment

In this chapter, the design of the experimental setup is presented. Also, the procedures of processing and analyzing the images are presented.

4.1 Test Experiments

Both direct and indirect methods of observing the wave patterns have been tested during the test experiments. In the direct methods, the wave pattern is directly observed on the water surface. In the indirect methods, the waves are observed indirectly by recording the refraction pattern below the wave. Four types of light are tested, a 1 kW tungsten lamp, a 55 W sodium lamp, a 10 W LED panel, and a 500 mW blue continuous laser sheet with a wavelength of 473 nm.

4.1.1 Direct methods

Figure (4.1.1) below shows images from five experimental setups using different lights when illuminating the tank by backlighting. The camera is placed above the center of the tank. The tank is filled with 5 cm clean tap water unless otherwise specified. The waves are generated by dropping a 1.6 cm diameter marble through a vertical tube at a distance of 27 cm above the bottom of the tank.

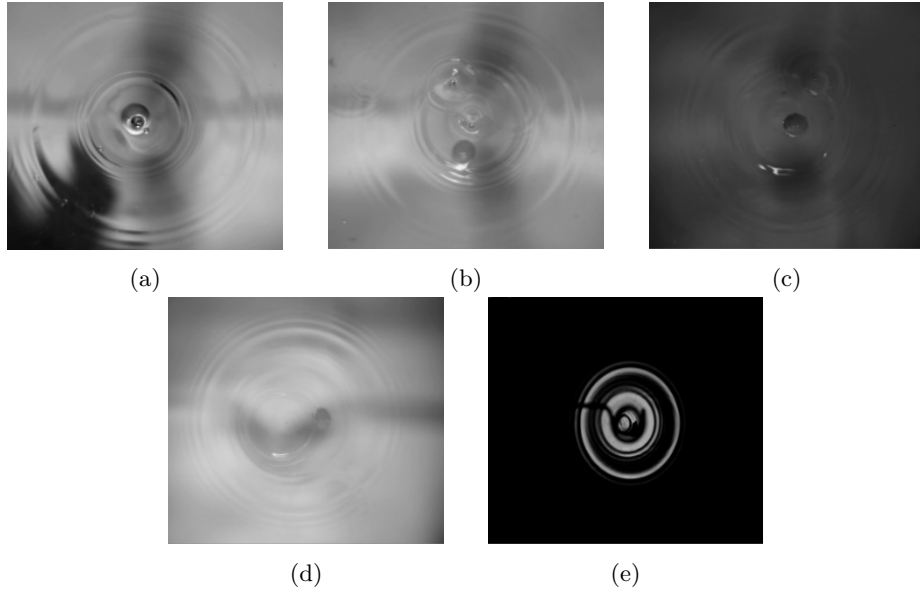


Figure 4.1.1: Directly observed waves generated by a 1.6 cm marble for five different setups. (a) 30° angled tungsten lamp. (b) 30° angled sodium lamp. (c) 30° angled sodium lamp, water diluted with blue food coloring. (d) Horizontal laser sheet. (e) Sodium lamp straight from below with sides of the tank covered by grey drafting paper.

The tank in setups 4.1.1a - 4.1.1c is placed directly on the floor. In the remaining setups, the tank is placed the same way as shown in Figure (4.2.1). In setup 4.1.1a, illuminating with the tungsten lamp leads to the problem of flickering when recording with a high-speed camera. Moreover, the setups 4.1.1a - 4.1.1d, inspired by Tavoularis, 2005, yield low-contrast images.

Furthermore, covering the tank with grey drafting paper, as in setup 4.1.1e increase the contrast. This setup, using a sodium lamp and covering the tank sides with grey drafting paper, illuminates a circular area with a diameter of 17 cm.

Two more setups for directly observing the surface waves are shown in Figure (4.1.2) below. For these setups, the tank is filled with 6 cm clean tap water.

Using a spherical reflector together with a LED-panel, as in setup 4.1.2a, expands the illuminated circular area to a diameter of 28 cm. However, the illuminated area created by the spherical reflector is not satisfactory homogeneous. Also, although the illuminated area is larger, compared with

setup 4.1.1e, the contrast of the waves decreases further out, making it possible to track the waves at an area with diameter of 17 cm.

Lastly, in setup 4.1.2b, the LED-panel together with a diffusor conducted by a 3 mm frosted acrylic sheet. This setup creates a more homogeneously lit area, compared with the aforementioned setup. This setup illuminates a circular area with a diameter of approximately 22 cm. Out of the setups tested, setup 4.1.2b yields the most homogenous illumination and the best contrasting images. To conclude, out of the setups tested, setup 4.1.2b yields the best results.

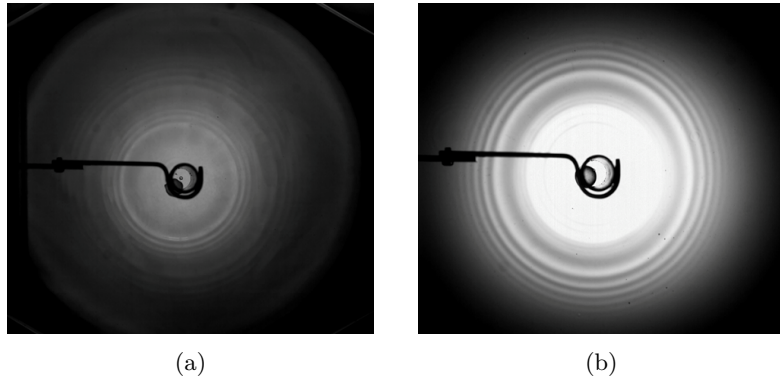


Figure 4.1.2: Directly observed waves generated by a 1.6 cm marble for two different setups. **(a)** Perpendicular LED-panel from below. With spherical reflector and a thin cloth as diffusor. **(b)** Perpendicular LED-panel from below. With acrylic sheet as diffusor.

The measurements for setup 4.1.2b, together with a sketch of the setup is found in Appendix A.

4.1.2 Indirect methods

Two indirect methods of observing the waves are tested and shown in Figure (4.1.3) below.

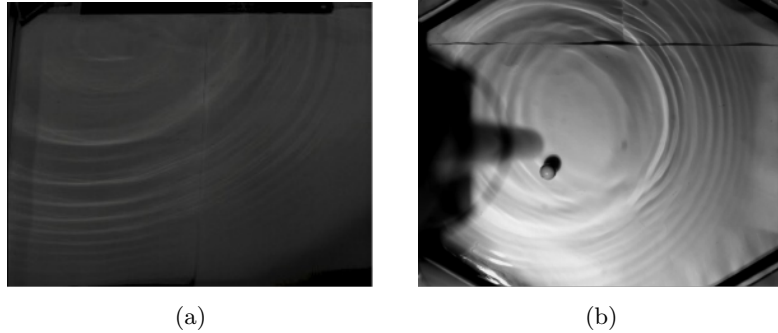


Figure 4.1.3: Indirectly observed waves generated by a 1.6 cm marble for two different setups. (a) Tungsten lamp straight from above. Camera placed at the side of the tank recording the floor below the tank. (b) Both Tungsten lamp and camera straight from above.

In setup 4.1.3a, the tank is placed in the same way as shown in Figure (4.2.1). The refraction pattern are recorded on a white drafting paper placed on the floor below the tank. This setup results in an unambiguous refraction pattern below the tank. Moreover, the tungsten light is not sufficient to yield good enough contrast.

Moreover, in setup 4.1.3b, the tank is placed directly on top of a white drafting paper on the floor. Recording the pattern below the wave in this way results in the water surface itself causing disturbances to the wave patterns.

Therefore the indirect methods were discarded due to their increased complexity and the poorer results yielded compared to the direct methods.

4.1.3 High speed camera

To capture the wave patterns, a MotionBLITZ EoSens mini - high speed camera was used together with the operator software MotionBLITZ Director2. The MotionBLITZ EoSens mini is equipped with a CMOS imaging sensor. The camera was centered 115 cm above the bottom of the tank. The wave patterns were recorded at a fixed framerate of 300 fps which enabled a resolution of 1024x1280 pixels.

To convert the measurements of wavelengths and wave speeds from units of pixels to meters, a reference length of known length, l , is placed horizontally at the water surface. A 30 cm steel ruler is used as a reference length and is measured in units of pixels from the image by the ruler tool in MATLAB Image Processing Toolbox. From this, a scaling factor can be formulated as

$$f = \frac{\sqrt{(x_1 - x_2)^2 + (y_1 - y_2)^2}}{l} , \quad (4.1)$$

where (x_1, y_1) and (x_2, y_2) are the pixel coordinates of the reference length edges.

4.1.4 Water depth

The maximum wavelength generated on the surface by a dropped object is typically a few times bigger than the object itself (Kundu et al., 2016). By plotting the inequalities for deep and shallow water from chapters 2.6.1 and 2.6.2, the required water depth of the tank for the different cases of interest can be decided.

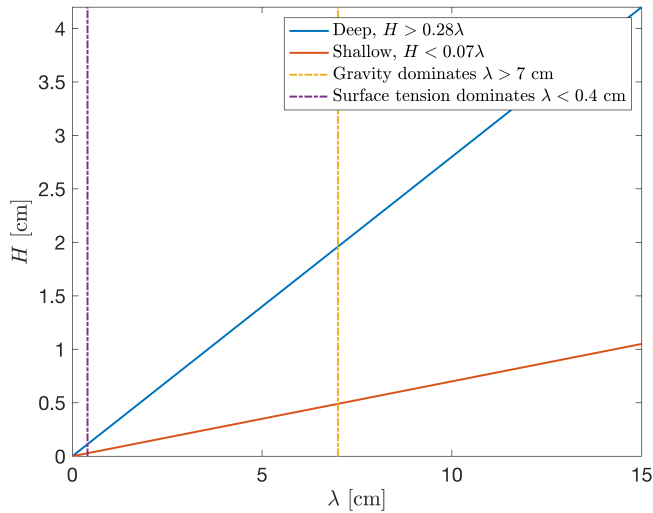


Figure 4.1.4: Inequality plot over water depth H vs wavelength λ for an air-water interface at $T = 20$ °C.

For an air-water interface at $T = 20$ °C, as mentioned in chapter 2.4.1, wavelengths longer than 7 cm are dominated by gravity with an accuracy of 3 %. This is shown by comparing the pure GW in eq. (2.24) with the CGW in eq. (2.30). Moreover, with an accuracy of 3 %, wavelengths < 4 mm are dominated by surface tension. This is shown by comparing the pure CW with the CGW in eq. (2.30).

4.1.5 Avoiding problems from reflections

Unwanted disturbances to the experiment, such as interference and standing waves, can occur from wave reflections at the wall. To avoid these reflections, the experiment is performed for a limited period so that the reflecting wave does not have time to return to the measurement area. To be able to perform the experiment for as long time as possible the disturbance object must not be too large due to the dispersive behavior of the wave. Other similar experiments (see

e.g. Scott, 1981; Taklo et al., 2015; Zhang, 1995) have used wave absorbers such as wave absorbing beaches to reduce wave reflections. To avoid that standing waves are generated in the water tank when dropping the object, the following wavelengths must be avoided (Kundu et al., 2016)

$$\lambda = \frac{2L}{(n+1)} , \quad n = 0, 1, 2, \dots \quad (4.2)$$

Here, L is the diameter of the water tank. Figure (4.1.5) below gives a graphical view for which wavelengths to avoid depending on the size of the tank.

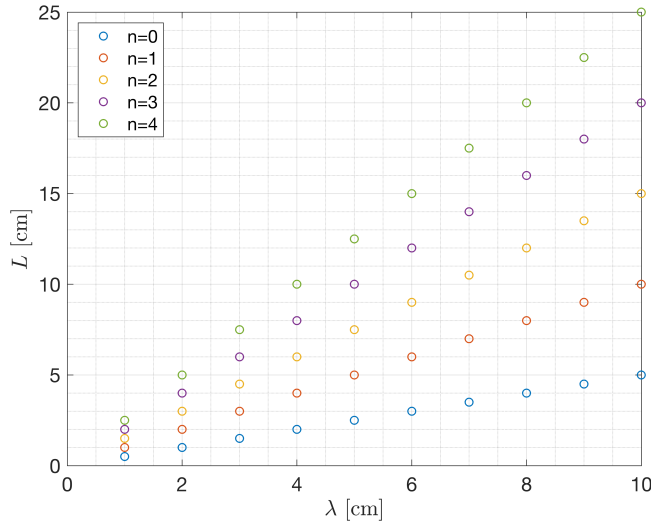


Figure 4.1.5: Tank size vs. wavelengths for which standing waves occur.

4.1.6 Problems due to splashes

Furthermore, unwanted disturbances from splashes may also occur when the stone hits the water. These splashes give rise to multiple unwanted wave sources, which can lead to constructive and destructive interference.

4.2 Experimental setup

A test experiment setup, shown in Figure (4.2.1) below, is used to evaluate which illumination method to use. To create the waves, a 1.6 cm diameter marble is dropped by hand through a plastic tube in the center of a 35 cm diameter hexagonal glass tank filled with 2–8 cm of water. The plastic tube is fixed with the dropping point at 27 cm above the bottom of the tank. Since the dropping point is stationary, the dropping-height increases with decreasing water depth.

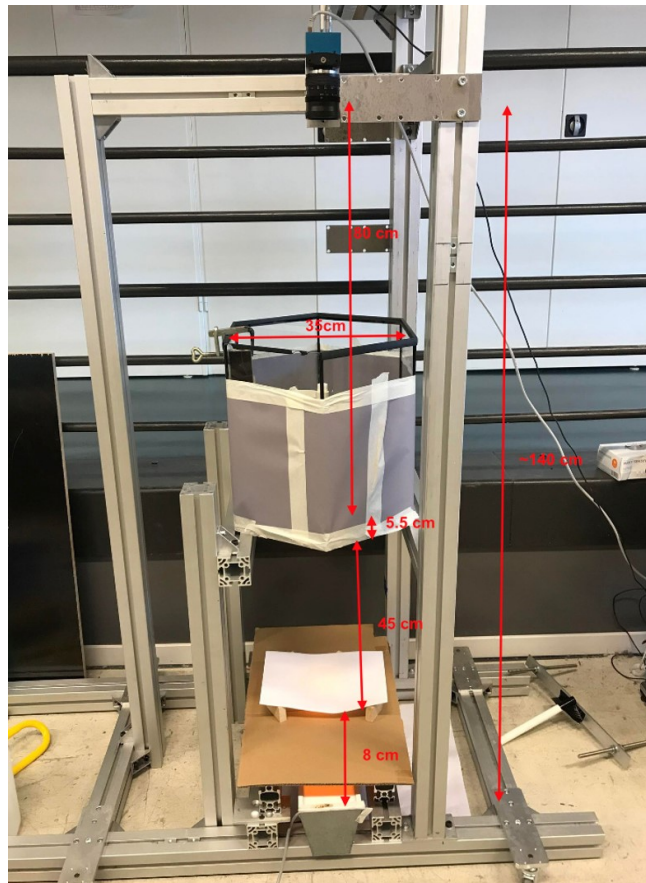


Figure 4.2.1: Test-experiment setup.

The tank is illuminated by back-lighting from below with an Osram 55 W sox sodium lamp, which is powered by a Phillips electronic SOX ballast EXC 055 S/50. A 3 mm thick white acrylic sheet covering the sodium lamp is used together with a white A4 writing paper as a diffusor.

Three different types of marbles, shown in Figure (4.2.2), are tested. The three types of materials were stone, glass, and hard plastic. All marbles are of the same size, with a diameter of 1.6 cm.



Figure 4.2.2: Three different types of marbles.

By testing three different marbles, the conclusion is made that the stone marbles are fragile and break after only a few tries, which leaves residue at the bottom of the tank. The marble made of glass had the issue that it bounced on the bottom of the tank and rolled away from the center. The plastic marble had the benefit of not bouncing as much. Moreover, the plastic marble did not roll away and remained in the center of the tank.

4.3 Image processing procedure

The following procedure, inspired by Li et al., 2019, is used to process the experimental images in MATLAB.

- Average image
- Background subtraction
- Adjust contrast
- Filter images using the MATLAB command imdiffusefilt:
- Threshold/binarize images
- Noise removal with the MATLAB commands bwareaopen: and imclearborder::

To reduce the background noise, the first 15 images in the batch are averaged and subtracted from all images. These images are taken before the object hits the water surface. The first steps of the procedure are shown in Figure (4.3.1) below.

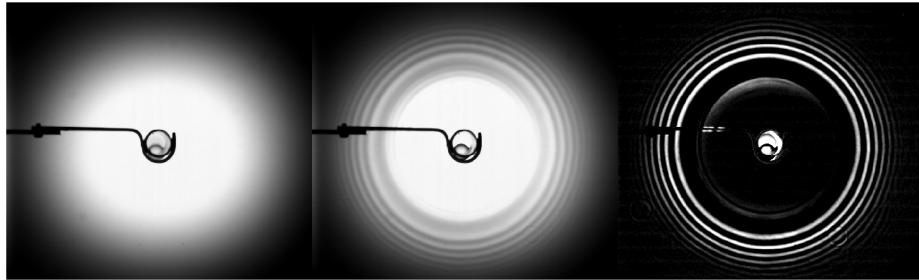


Figure 4.3.1: Background image (left). Original image (center). Background subtracted image (right).

Further processing steps are needed to get rid of the noise. When binarizing the images, a suitable threshold for pixel intensities is found by trial and error. The threshold must be set low enough to avoid erasing the outermost, darker wave patterns. Also, the threshold must be set high enough to eliminate unwanted noise from, e.g., secondary wave sources created by droplets. A suitable threshold depends on the brightness of the illumination. Lastly, the MATLAB functions `bwareaopen`: and `imclearborder`: are used to clean up residual pixels. The function `bwareaopen`: does this by removing objects consisting of fewer pixels than a selected threshold from the binary image. Moreover, `imclearborder`: removes objects from an image that are brighter than their surroundings and are connected to the image border.

4.4 Measuring the wave speed

Figure (4.4.1) below illustrates the difference in wave patterns generated by a big and a small object, here represented by the classical example stone vs. droplet, respectively. The figure illustrates how the waves propagate in the radial direction, and the contours represent individual wave crests. Gravity is the dominant restoring force giving rise to the wave pattern in Figure (4.4.1a). In contrast, surface tension is the dominant restoring force giving rise to the wave pattern in Figure (4.4.1b).

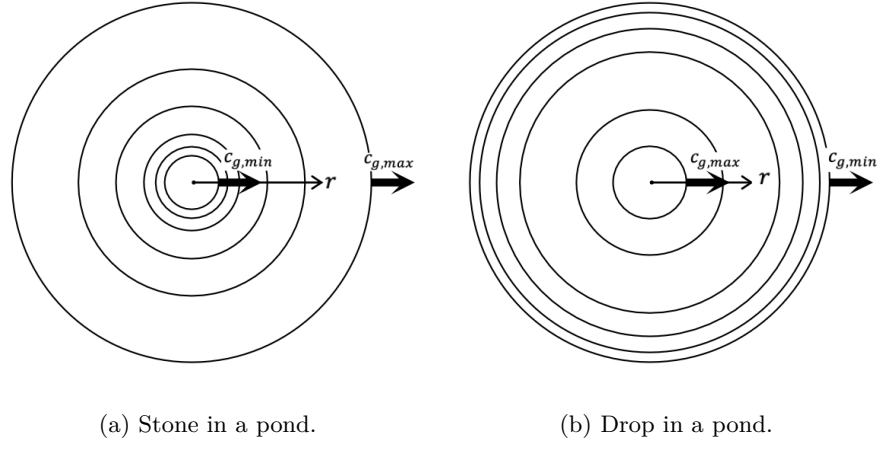


Figure 4.4.1: Illustrations of the wave patterns formed by dropping a stone and a droplet in a deep pond.

By measuring the radial position of the wave crest at two different instances in time, as illustrated in Figure (4.4.2), it is possible to experimentally determine the wave speed according to

$$c_{wave} = \frac{\Delta r}{\Delta t} = \frac{r_{i+1} - r_i}{\Delta t} . \quad (4.3)$$

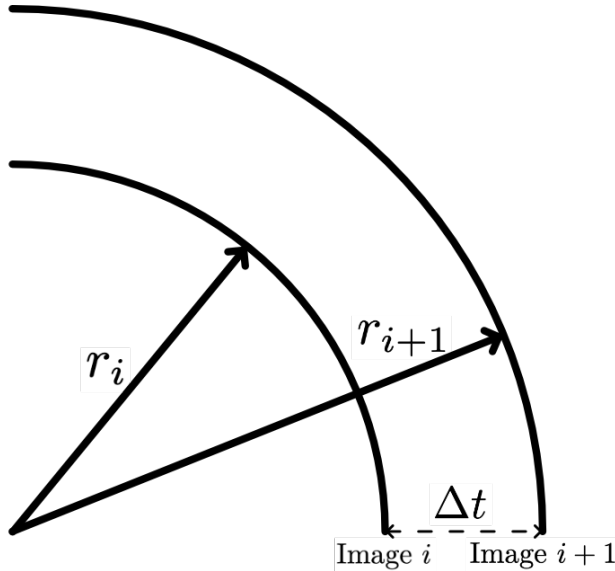


Figure 4.4.2: Illustration of the change in radial position for one wave crest at the fixed time interval, Δt , between two images.

4.4.1 Wave tracking

To track the wave crests, the binarized images are analysed both vertically and horizontally around $y = y_0 \pm 10$ px and $x = x_0 \pm 10$ px respectively. Firstly, to find the origin of the wave pattern, (x_0, y_0) , the MATLAB function `imfindcircles` is used. Secondly, in the binarized images, the positions of the crests, x_i and y_i , are found by using the `regionprops` function and finding centroids of the pixel objects in each binarized image. This is shown in Figure (4.4.3) below.

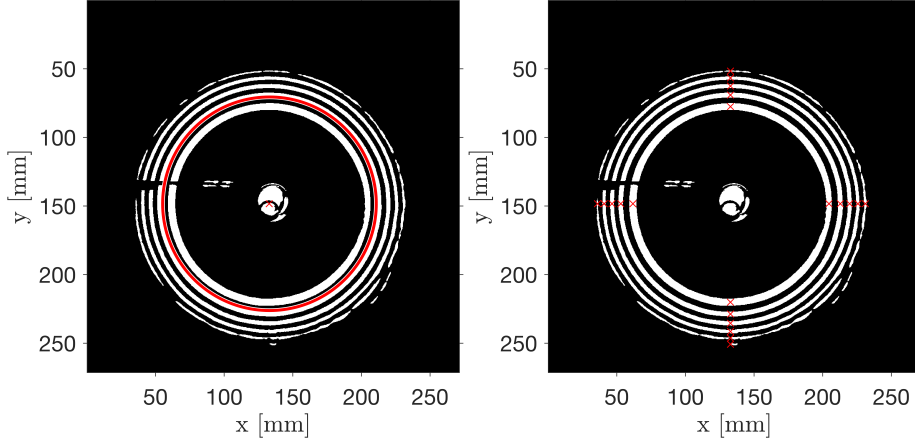


Figure 4.4.3: Finding the wave pattern origin with `imfindcircles` (left). Finding and highlighting crest positions horizontally and vertically. (right). Wave patterns generated by a 1.6 cm marble dropped in 6 cm deep water.

The waves are tracked outward from the wave origin in four directions, positive and negative x -direction, and positive and negative y -direction. For the positive and negative x -directions, the absolute radial distances to the crests are given by

$$r_i = |x_i - x_0| \quad , \quad i = 1, 2, 3, \dots . \quad (4.4)$$

Here, x_i is the x -coordinate of crest number i counted outward from the wave center.

For the positive and negative y -directions, the absolute radial distances to the crests are given by

$$r_i = |y_i - y_0| \quad , \quad i = 1, 2, 3, \dots . \quad (4.5)$$

Here, y_i is the y -coordinate of crest number i counted outward from the wave center.

Taking the temporal difference of the radii, as in eq. (4.3) gives the phase speed of the wave. Since the images are recorded at a fixed framerate of 300 fps, the time step between two images is fixed at $\Delta t = 1/300 = 0.0033$ s.

Furthermore, the absolute value wavelengths, λ_i , is given by the spatial difference of the radii

$$\lambda_i = |r_{i+1} - r_i| . \quad (4.6)$$

This is implemented in MATLAB as shown in Figure (4.4.4) below.

```
% Calculating lambda and dR
Lambda = cellfun(@(r) abs(diff(r)), R, 'UniformOutput',false);
Lambda(cellfun(@isempty,Lambda)) = {nan};

%Calculating dR
dR = cell(t2-t1,2);
for i = 1:(t2-t1)
    for j = 1:4
        if numel( R{i,j} ) == numel( R{i+1,j} )
            dR{i,j} = abs(R{i+1,j} - R{i,j});
        else
            dR{i,j} = [];
        end
    end
end
dR(cellfun(@isempty,dR)) = {nan};
```

Figure 4.4.4: MATLAB code for calculations of wavelength and temporal difference of the radii.

In Figure (4.4.4), $r = R(t)$, i.e., The radial positions measured at time t . Moreover, the MATLAB cell array dR : in Figure (4.4.4) stores the wave crest data in four columns, $j = 1 : 4$. $j = 1 : 2$ constitute wave crests traveling in the positive and negative x -direction, respectively. $j = 3 : 4$ constitute wave crests traveling the in positive and negative y -direction, respectively.

Chapter 5

Results

In this chapter, the experimental results and the associated normalized absolute errors are presented. Furthermore, in order to evaluate the tank size, results from placing the LED-panel off-center is presented in section 5.1.

All experiments is conducted under the same conditions. With water temperature measured to be 22 °C. At this temperature, the surface tension is $72.75 \cdot 10^{-3}$ N/m according to (Vargaftik et al., 1983). The scaling factor, f , was calculated to $3.040 \cdot 10^{-4}$. The images are recorded at a fixed framerate of 300 fps.

5.1 Results from the marble

Figure (5.1.1) show the unaltered image and the resulting processed image.

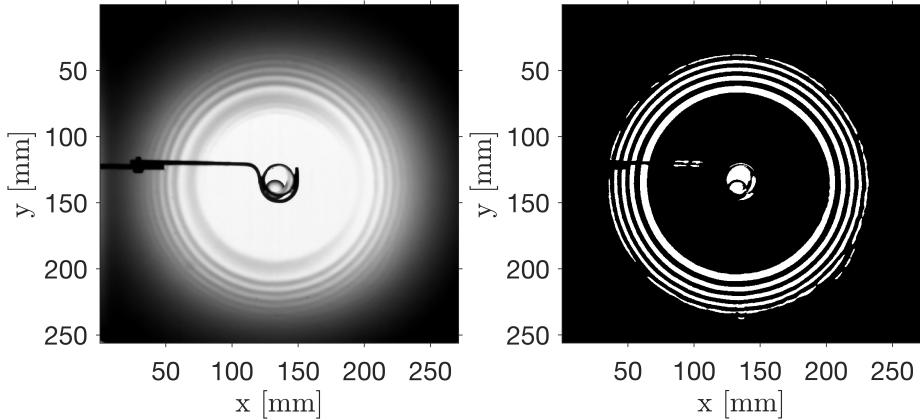


Figure 5.1.1: Original image (Left). Filtered and thresholded image (Right). For water depth 6 cm.

The experimental results from dropping a 1.6 cm diameter marble in the tank filled with water at the depths of 1, 6, and 10 cm are presented in Figure (5.1.2) below. The results in Figure (5.1.2) are presented together with the averaged phase speed values on wavelength intervals of 0.1 cm, represented by the red bullets.

In section 4.1.4, it was mentioned that the maximum wavelength generated by an object is a few times larger than the object itself. By assuming the maximum wavelength generated by the marble is five times larger than the marble itself, the expectation is to see wavelengths up to 8 cm. By recalling Figure (4.1.4), the expectation is that water depths of 6 and 10 cm will show a deep-water CGW behavior. For the case with a water depth of 1 cm, the expectation is neither a deep nor shallow water behavior but an intermediate water depth CGW behavior according to equation (2.30). Only for the largest wavelengths a pure deep-water GW behavior is expected.

CHAPTER 5. RESULTS

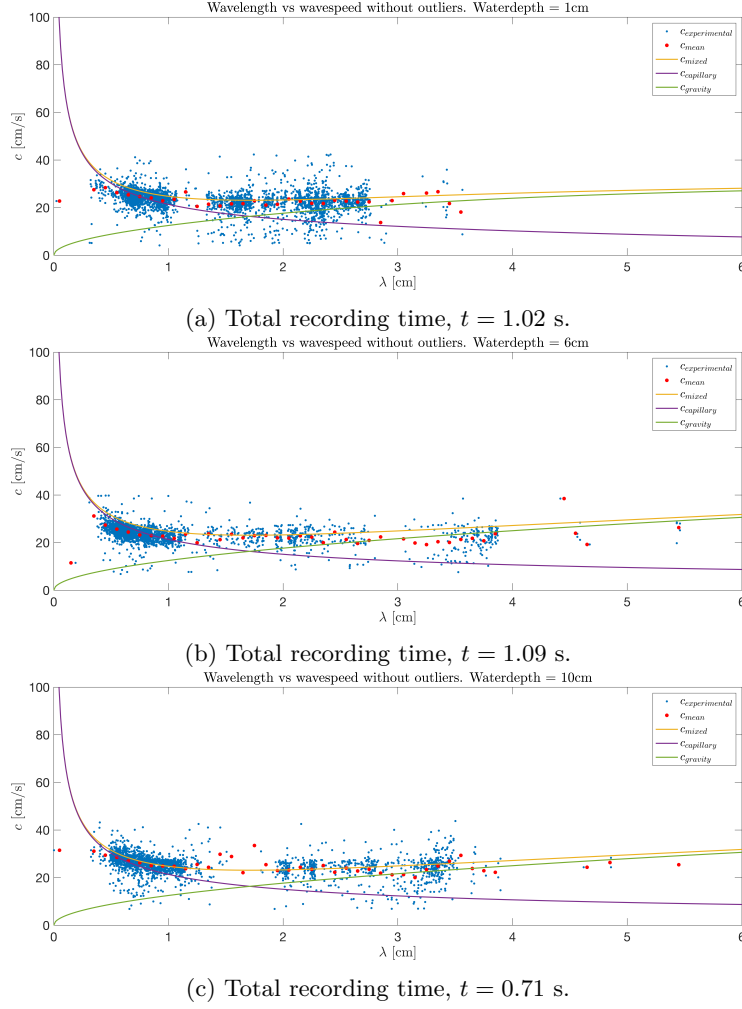


Figure 5.1.2: Results for dropping a 1.6 cm marble. Data recorded from one realisation for each water depth. Red bullets represent the averaged data on λ intervals of 0.1 cm.

The averaged data from the three water depths, 1, 6, and 10 cm, are presented in Figure (5.1.3) to elucidate the effects of H .

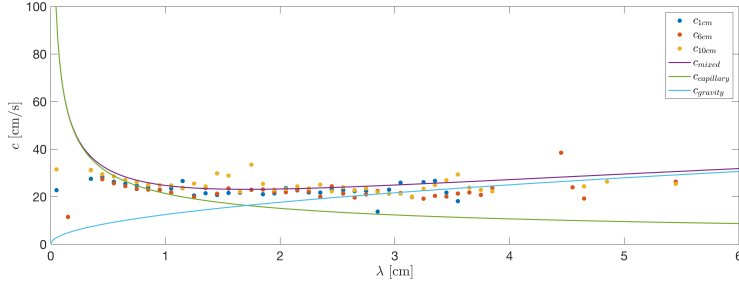


Figure 5.1.3: Averaged results from dropping a 1.6 cm marble. Averaged phase speed data on λ intervals of 0.1 cm for water depths 1, 6, and 10 cm.

Figure (5.1.3) shows that H does not affect the result, indicating that the water is always deep. This is also supported by the statement in chapter 2.6.1, that the deep-water approximation hold, with a 3% accuracy, for $H > 0.28\lambda$. For the largest captured wavelengths, $\lambda = 3.5$ cm, $0.28\lambda = 0.98$ cm, i.e. less than H for water depth 1 cm.

In chapter 2.4.1, it is mentioned that under room temperature conditions, $T = 20^\circ\text{C}$, there is a minimum wavelength, $\lambda_{min} = 1.71$ cm, yielding a minimum wave speed of $c_{min} = 23.1$ cm/s. Looking at the averaged results in Figure (5.1.3), for $\lambda = 1.7$ cm, the wavespeed is 24.2 cm/s.

The associated normalized absolute errors, defined in eq. (5.1), are presented in Figure (5.1.4) below.

$$\epsilon = \frac{|c_{experimental} - c_{theory}|}{c_{theory}} \quad (5.1)$$

CHAPTER 5. RESULTS

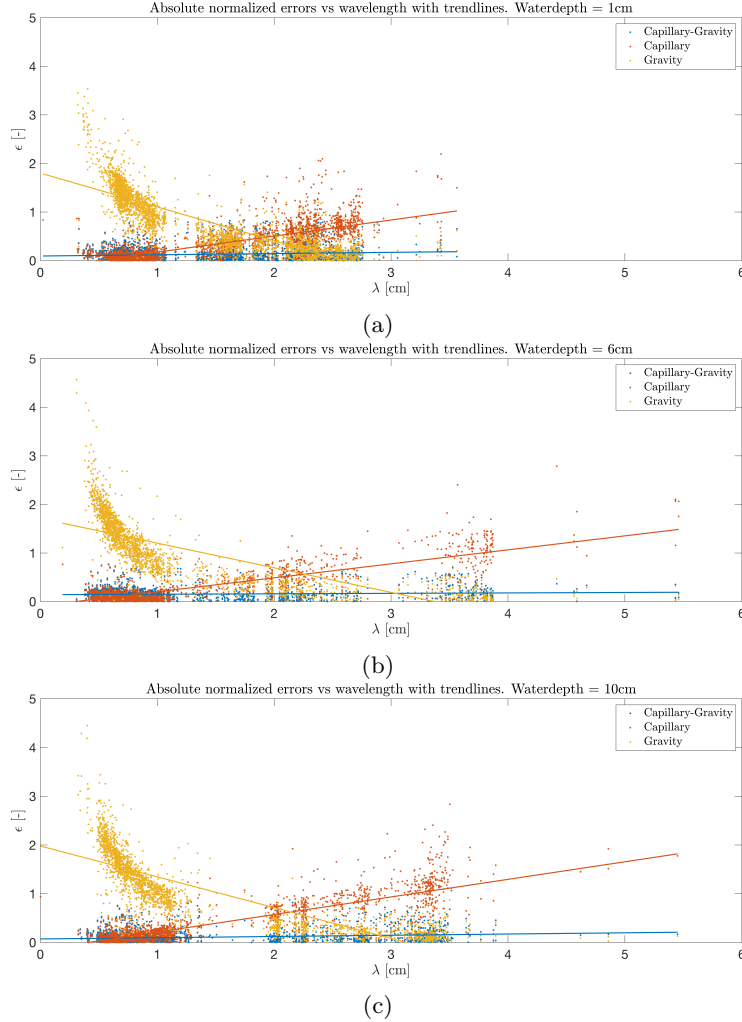


Figure 5.1.4: Normalized absolute errors for dropping a marble. The solid lines correspond to the linear trend of the scattered data of matched color, respectively.

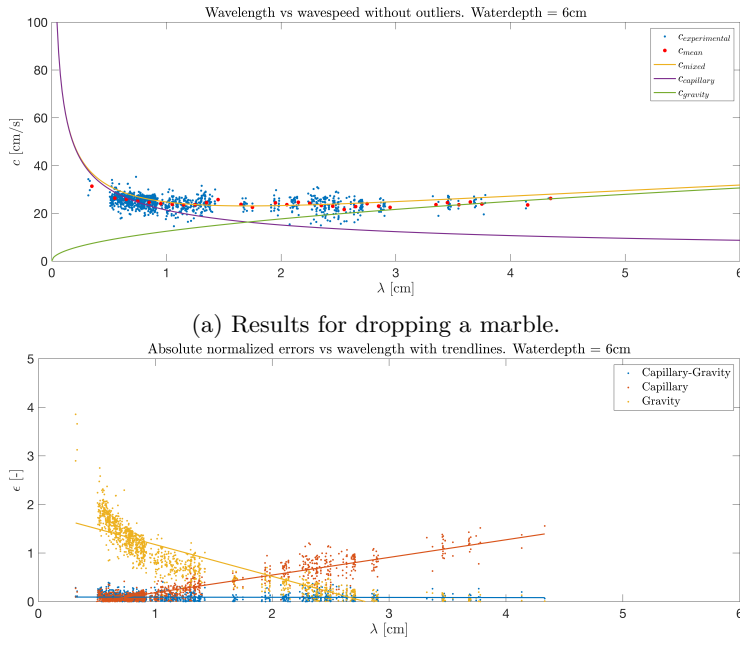
Looking at the errors presented in Figure (5.1.4), the capillary-gravity case errors are approximately constant over the entire wavelength range. For water depth of 1 cm, the mixed case errors are approximately 14%. The errors decrease when the water depth increase. For a water depth of 6 and 10 cm, the errors are approximately 13% and 11%, respectively.

One thing to note is the behavior of the trendlines for the pure gravity and pure capillary cases, respectively. The pure gravity case errors increase for decreasing wavelengths. The opposite is true for the pure capillary case, for which the error

CHAPTER 5. RESULTS

increases for increasing wavelengths. Looking at the intersection between the pure gravity and pure capillary error trendlines in Figure (5.1.4a) - (5.1.4c). For a water depth of 1 cm, the intersection occurs at $\lambda \approx 1.9$ cm. For water depths of 6 and 10 cm, the intersections occur at $\lambda \approx 2.2$ cm.

The LED used in the experiment is not sufficient to illuminate the entire area of the tank. To investigate if the maximum wavelengths measured are limited by the tank size or by the 1.6 cm diameter marble the LED is moved off-center. Moving the illumination off-center of the tank allows for illumination from the center of the tank, to the wall on the right-hand side. If the maximum wavelengths are limited by the size of the tank, moving the LED off-center is expected to show longer wavelengths. In Figure (5.1.5), the experimental results from moving the LED-panel off-center are presented.



(b) Normalized absolute errors for dropping a marble.

Figure 5.1.5: Results from dropping a 1.6 cm marble in 6 cm water. LED-panel positioned off-center to allow for illumination of one side. Red bullets in (a) represent the averaged data on λ intervals of 0.1 cm. Total recording time, $t = 0.96$ s.

Figures (5.1.2b), (5.1.2c), and (5.1.5a) shows that the generated wavelengths range between approximately 0.4–3.5 cm. This differs from the expected wavelength range, up to about 8 cm. Since the maximum wavelength, captured in the off-center case in Figure (5.1.5a), is about 3.5 cm, this indicates that the

marble's size is the limiting factor, not the tank's size. Figures 5.1.4 and 5.1.5b show that the capillary-gravity case-errors are approximately constant over the entire wavelength range, indicating a CGW behavior over the entire wavelength range. This is as expected beforehand since the pure deep-water GW behavior was only expected for wavelengths above 7 cm.

5.2 Results from the droplet

Figure (5.2.1) show the unaltered image and the resulting processed image.

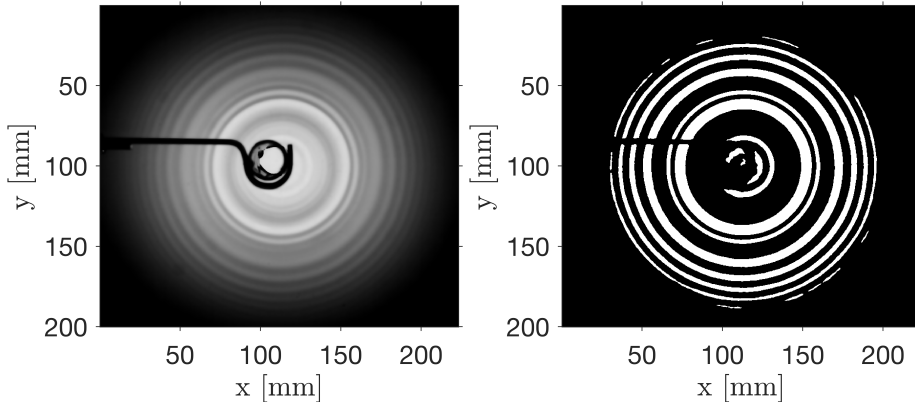


Figure 5.2.1: Original image (Left). Filtered and thresholded image (Right). For water depth 6 cm.

The experimental results from dropping a water droplet in the tank, filled with water at the depths of 1, 3, and 6 cm are presented in Figure (5.2.2) below. The results in Figure (5.2.2) are presented together with the averaged phase speed values on wavelength intervals of 0.1 cm, represented by the red bullets.

The experimental setup for dropping the water droplet differs in one aspect from what is described in section 4.2. Instead of releasing the object by hand through the fixed plastic tube, the object is released via a pipette through the fixed plastic tube. Since the plastic tube is fixed, the dropping height increases with decreasing water depth. The diameter of the droplet is estimated to 4 mm.

In section 4.1.4, it was mentioned that the maximum wavelength generated by an object is a few times larger than the object itself. Assuming the maximum wavelength generated by the droplet is five times larger than the droplet itself, the expectation is to see wavelengths up to 2 cm. By recalling Figure (4.1.4), the expectation is that all three cases expect to show the same deep-water CGW

CHAPTER 5. RESULTS

behavior. For the smallest wavelengths, a pure deep-water CW behavior is expected.

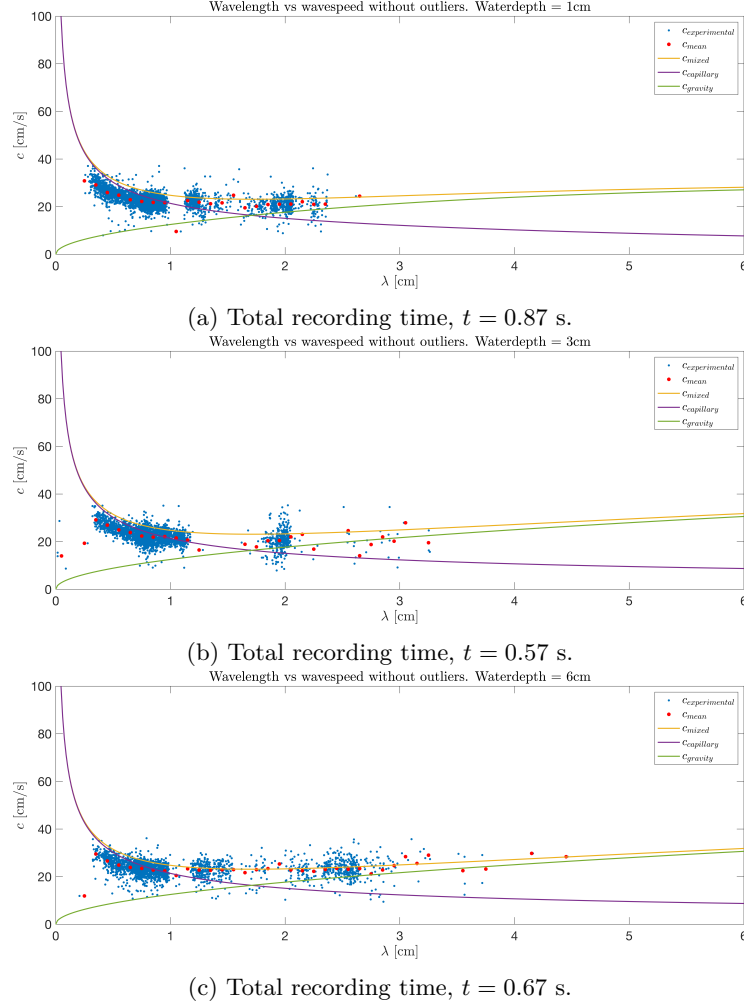


Figure 5.2.2: Results for dropping a 4 mm water droplet. Data recorded from one realisation for each water depth. Red bullets represent the averaged data on λ intervals of 0.1 cm.

The averaged data from the three water depths, 1, 3, and 6 cm, are presented in Figure (5.2.3) to elucidate the effects of H .

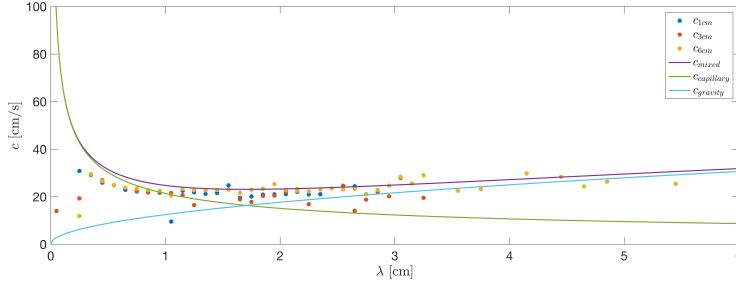


Figure 5.2.3: Averaged results from dropping a 4 mm droplet. Averaged phase speed data on λ intervals of 0.1 cm for water depths 1, 3, and 6 cm.

Figure (5.2.3) shows that H does not affect the result, indicating that the water is always deep. This is also supported by the statement in chapter 2.6.1, that the deep-water approximation hold, with a 3% accuracy, for $H > 0.28\lambda$. For the largest captured wavelengths, $\lambda = 2.5$ cm, $0.28\lambda = 0.7$ cm, i.e. less than H for water depth 1 cm.

In chapter 2.4.1, it is mentioned that under room temperature conditions, $T = 20$ °C, there is a minimum wavelength, $\lambda_{min} = 1.71$ cm, yielding a minimum wave speed of $c_{min} = 23.1$ cm/s. Looking at the averaged results in Figure (5.2.3), for $\lambda = 1.7$ cm, the wavespeed is 19.1 cm/s.

The associated normalized absolute errors, defined in eq. (5.1), are presented in Figure (5.2.4) below.

CHAPTER 5. RESULTS

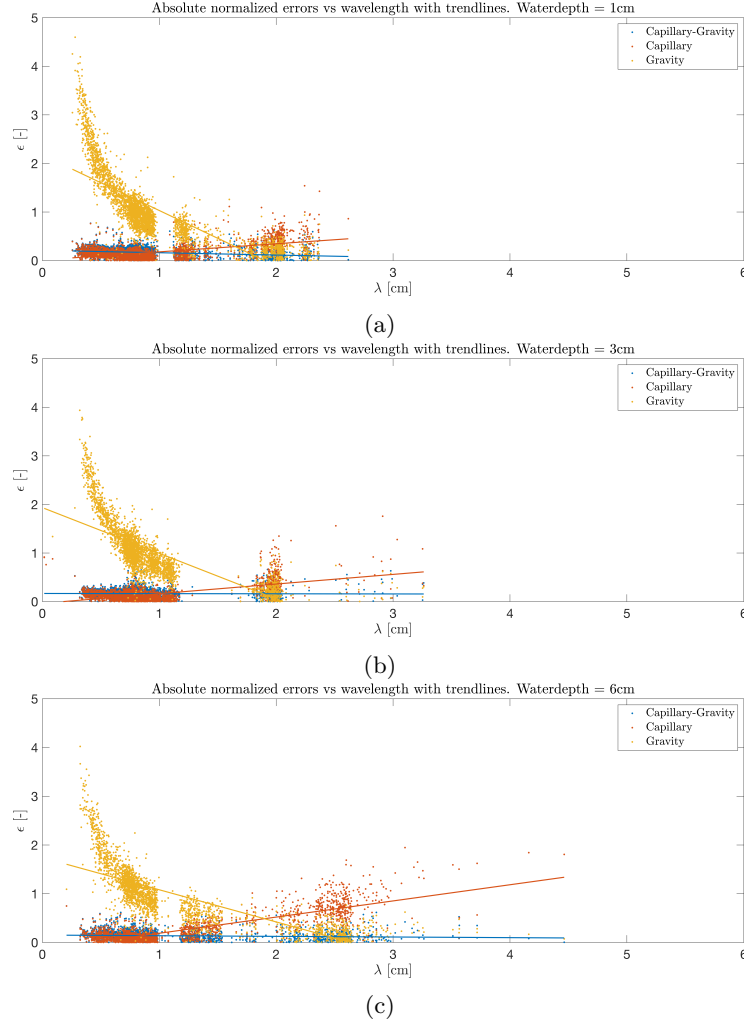


Figure 5.2.4: Normalized absolute errors for dropping a water droplet. The solid lines correspond to the linear trend of the scattered data of matched color, respectively.

Looking at the errors presented in Figure (5.2.4). For a water depth of 1 cm, the mixed case errors are decreasing for increasing wavelengths. In Figure (5.2.4a), the mixed case errors range between 8–20%, with an average error of 14%. For water depths of 3 and 6 cm, the capillary-gravity case errors are approximately constant over the entire wavelength range, with errors of 16% and 12%, respectively.

One thing to note is the behavior of the trendlines for the pure gravity and pure

CHAPTER 5. RESULTS

capillary cases, respectively. The pure gravity case errors increase for decreasing wavelengths. The opposite is true for the pure capillary case, for which the error increases for increasing wavelengths. Looking at the intersection between the pure gravity and pure capillary errors trendline in Figure (5.2.4a) - (5.2.4c). For a water depth of 1 cm, the intersection occurs at $\lambda \approx 1.7$ cm. For water depths of 3 and 6 cm, the intersections occur at $\lambda \approx 1.8$ cm and 1.9 cm, respectively.

Figure (5.2.2) show that the generated wavelengths range between approximately 0.4–2.5 cm. This agrees with the expected wavelength range, up to about 2 cm. Figure (5.2.4) show that the capillary-gravity case-errors are approximately constant over the entire wavelength range, indicating a CGW behavior over the entire wavelength range. This is as expected beforehand since the pure deep-water CW behavior was only expected for wavelengths below 0.4 cm.

Chapter 6

Discussion

6.1 Sources of uncertainty

In this section, the sources of uncertainty are discussed.

6.1.1 Water depth and noise

Looking at the results from dropping the marble, in Figure (5.1.2), the shallow-water data, 1 cm, are noisier compared to the data collected at 6 and 10 cm water depth. There are two reasons for this. Firstly, since the dropping point is stationary, the dropping-height increases with decreasing water depth. This increased dropping height leads to more splashes at the impact, which creates unwanted wave sources. Secondly, in deeper water, the marble slows down through the water before hitting the bottom of the tank. Therefore, the marble does not bounce as much in deep water compared to shallow water.

6.1.2 Errors due to illumination

Looking at Figure (5.1.2b), for wavelengths of 3.5 cm, the wave speed varies between $\approx 10 - 35$ cm/s. One reason for the same wavelength having multiple wave speeds may be that the illumination is not perfectly perpendicular to the water surface. Causing the light to refract differently on the right-hand side compared to the left-hand side of the center of the wave.

6.1.3 Errors due to image processing

A problem arises when tracking waves over time from a sequence of about 200 images. Two problems are connected to the image processing step. The two problems are connected to the choice of the threshold used to binarize the images. Firstly, if the threshold is set too low, there is a risk of finding false

wave crests in the form of unwanted noise in the processed images. Secondly, if the threshold is set to high, there is a risk of removing and missing true wave crests.

Looking at the filtered and thresholded image at the right in Figure (5.1.1), there is unfiltered noise at the outermost edge. Moreover, the innermost crest appears only above the center and is missing a large part of its circumference.

Another source of error when tracking the wave crests arises when the leading crests reach the edge of the illuminated region. Reaching the edge makes the crest width go thinner and eventually disappear. This phenomenon makes the virtual crest-center appear to stand still instead of continuing forward.

6.2 Short and long wavelengths

From the figures (5.2.2) and (5.1.2), it appears that the wavelengths range between ≈ 0.4 – 2.5 cm for the droplet. And about ≈ 0.4 – 3.5 cm for the marble. Most of the cases in the figures show there are few data points for wavelengths $\lesssim 0.4$ cm, one explanation for this could be that smaller waves scatter light less than big waves and therefore has lower contrast when recorded.

However, for wavelengths in the upper range, ≈ 3.5 cm for the marble and ≈ 2.5 cm for the droplet. It is more difficult to conclude if the wavelength upper limit is because these are the longest wavelengths produced by the objects; alternatively, if the wavelength upper limit is due to the size of the water tank being too small. The results in Figure (5.1.5a.), generated by an off-center positioned LED-panel show the maximum wavelength recorded to be approximately 3.5 cm. This is also the maximum wavelength for the results generated by a center position LED, as in Figure (5.1.2b).

Furthermore, looking at the wave pattern generated by the droplet in 6 cm deep water in Figure (5.2.1), the wavelengths at the trailing wave crests are longer than the leading crests wavelengths. Comparing this to the deep-water case illustrations in Figure (4.4.1), it looks like surface tension is the dominating restoring force when disturbing the surface by dropping a 4 mm droplet. Moreover, looking at the wave pattern generated by the 1.6 cm marble in 6 cm deep water in Figure (5.1.1), the wavelengths at the trailing wave crests are, similar to the aforementioned case with the droplet, also longer than the leading crests wavelengths. Suggesting that surface tension is the dominating restoring force when disturbing the surface by dropping a 1.6 cm marble as well.

Chapter 7

Conclusions

The conclusion from this project is that it is possible to track surface waves and quantitative measure phase speed and wavelengths with the experimental setup designed during the project. However, the setup is not sufficient for reproducing the entire diagram shown in Figure (2.4.2). In chapter 6.2, it is mentioned that the shortest wavelengths recorded are ≈ 0.4 cm for both the marble and the droplet. Suggesting the setup is only sufficient for reproducing parts of the diagram for wavelengths $\gtrsim 0.4$ cm.

Comparing the wave pattern generated by the marble in 6 cm deep water in Figure (5.1.1) to the deep-water case illustrations in Figure (4.4.1), it looks like surface tension is the dominating restoring force when disturbing the surface by dropping a 1.6 cm marble. This indicates that a larger marble is needed to generate gravity-dominated waves.

Figures (5.1.3) and (5.2.3) show that H does not affect the result, indicating that the water is deep in all cases tested for both the marble and the droplet. This is supported by the statement in chapter 2.6.1, that the deep-water approximation hold, with a 3 % accuracy, for $H > 0.28\lambda$. For the largest captured wavelengths, $\lambda = 3.5$ cm, $0.28\lambda = 0.98$ cm, i.e., less than H for water depth 1 cm.

In chapter (4.1.4), it was mentioned that the maximum wavelength generated on the surface by a dropped object is typically a few times bigger than the object itself. The 1.6 cm marble generates wavelengths up to 3.5 cm, i.e., the marble generates wavelengths 2.2 times larger than the marble itself. Moreover, the 0.4 cm droplet generates wavelengths up to 2.4 cm, i.e., the droplet generates wavelengths 6.3 times larger than the droplet itself. Assuming that all spherical objects generate waves with the same scaling factor, this suggests that the illuminated area is too small for the waves generated by the marble to be fully developed.

In chapter (3.2.1), it is mentioned that flickerless illumination can be produced

by backlighting high-intensity LED lights through a diffusor made of thin drafting paper. However, since the purpose of using high-intensity LED is to eliminate flickering, the same result can be achieved by using a 10 W continuous LED-panel. Moreover, the use of a thin drafting paper as a diffusor, as in setup 4.1.1e, yields homogenous illuminated images, however, cluttered with paper fibers. In contrast, the 3 mm frosted acrylic sheet used in setup 4.1.2b also yields homogenous illumination. However, it does not have problems with noisy paper fibers in the background as in the aforementioned setup.

Hence, to capture wavelengths above 4 cm, the scale of the setup must be increased. To generate larger wavelengths, the object dropped must be increased. Which leads to the tank size must be increased. To illuminate a larger tank, more light is needed. To record a larger tank, the FOV need to be increased further by elevating the camera. In the setup, one LED-panel illuminates a circle with a diameter of approximately 22 cm. The LED has the measurements $15.1 \times 5.6 \times 10$ cm. To illuminate a circle with a diameter of 50 cm there needs to be 3×4 LED-panels placed side by side. To increase the camera FOV to a 50 cm diameter, the camera height must be increased to 140 cm.

In chapter 4.1.5, it is mentioned that other experiments, similar to the experiment in this project, have used wave absorbers such as wave-absorbing beaches to reduce wave reflections. Reflecting waves are not an issue for the experimental setup described in this project because the illuminated area is smaller than the tank area. I.e., the trailing edge wave reaches and disappears at the edge of the illuminated area before the reflection of the leading edge wave reaches back. However, if the illuminated area is equal to the tank area, wave-absorbing beaches may be used to prolong interference-free tracking of the trailing edge wave crest.

7.1 Future Work

For future work, to release the marble in a more controlled way, a recommendation is to construct a releasing mechanism. A simple idea for this release mechanism is to attach a release pin to the fixture holding the dropping pipe, see sketch in Appendix A. The marble is released by pulling the pin outward by hand.

Moreover, the experimental setup enables the further study of interference patterns caused by the interactions between the outward moving waves and the waves reflected from the side of the tank.

Furthermore, the experimental setup makes it possible to study the relation between the dropped objects kinetic energy and the splash zone generated at the impact.

Finally, since this study focused on linear surface waves an interesting field for

CHAPTER 7. CONCLUSIONS

future work would be to study the non-linear behavior of the surface waves closely after the impact.

References

- Acheson, D. J. (1990). *Elementary fluid dynamics*. Clarendon.
- Çengel, Y. A. (2015). *Heat and mass transfer: Fundamentals and applications* (5th ed. in SI units.). McGraw-Hill.
- Craeye, C., Sobieski, P., Bliven, L., & Guissard, A. (1999). Ring-waves generated by water drops impacting on water surfaces at rest. *Oceanic Engineering, IEEE Journal of*, 24, 323–332. <https://doi.org/10.1109/48.775294>
- Kundu, P. K., Cohen, I. M., & Dowling, D. R. (2016, January 1). Chapter 8 - gravity waves. In P. K. Kundu, I. M. Cohen, & D. R. Dowling (Eds.), *Fluid mechanics (sixth edition)* (pp. 349–407). Academic Press. <https://doi.org/10.1016/B978-0-12-405935-1.00008-3>
- Li, G., Agir, M. B., Kontis, K., Ukai, T., & Rengarajan, S. (2019). Image processing techniques for shock wave detection and tracking in high speed schlieren and shadowgraph systems [Publisher: IOP Publishing]. *Journal of Physics: Conference Series*, 1215(1), 012021. <https://doi.org/10.1088/1742-6596/1215/1/012021>
- Råde, L. (2004). *Mathematics handbook for science and engineering* (5., [rev.] ed.). Studentlitteratur.
- Scott, J. C. (1981). The propagation of capillary-gravity waves on a clean water surface. *Journal of Fluid Mechanics*, 108, 127–131. <https://doi.org/10.1017/S0022112081002024>
- Strickland, S. L., Shearer, M., & Daniels, K. E. (2015). Spatiotemporal measurement of surfactant distribution on gravity–capillary waves [Publisher: Cambridge University Press]. *Journal of Fluid Mechanics*, 777, 523–543. <https://doi.org/10.1017/jfm.2015.352>
- Ströbel, B. (2011). Demonstration and study of the dispersion of water waves with a computer-controlled ripple tank [Publisher: American Association of Physics Teachers]. *American Journal of Physics*, 79(6), 581–590. <https://doi.org/10.1119/1.3556140>
- Taklo, T. M. A., Trulsen, K., Gramstad, O., Krogstad, H. E., & Jensen, A. (2015). Measurement of the dispersion relation for random surface gravity waves [Publisher: Cambridge University Press]. *Journal of Fluid Mechanics*, 766, 326–336. <https://doi.org/10.1017/jfm.2015.25>

REFERENCES

- Tavoularis, S. (2005). *Measurement in fluid mechanics*. Cambridge University Press.
- Tropea, C., Yarin, A., & Foss, J. F. (2007). *Springer handbook of experimental fluid mechanics* (1st ed. 2007..). Springer Berlin Heidelberg.
- Vargaftik, N. B., Volkov, B. N., & Voljak, L. D. (1983). International tables of the surface tension of water [Publisher: American Institute of Physics for the National Institute of Standards and ...]. *Journal of Physical and Chemical Reference Data*, 12(3), 817–820.
- Zhang, X. (1995). Capillary–gravity and capillary waves generated in a wind wave tank: Observations and theories [Publisher: Cambridge University Press]. *Journal of Fluid Mechanics*, 289, 51–82. <https://doi.org/10.1017/S0022112095001236>
- Zou, J., Ren, Y., Ji, C., Ruan, X., & Fu, X. (2013). Phenomena of a drop impact on a restricted liquid surface. *Experimental Thermal and Fluid Science*, 51, 332–341. <https://doi.org/10.1016/j.expthermflusci.2013.08.016>

Appendix - Contents

A First Appendix	50
------------------	----

Appendix A

First Appendix

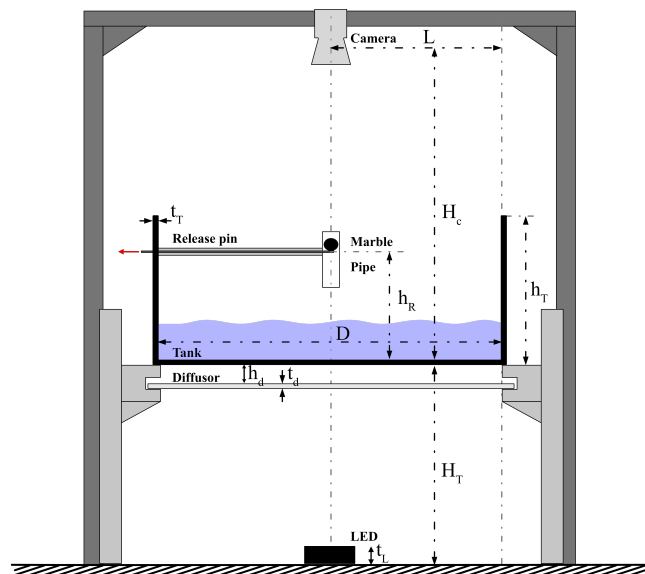


Figure A.0.1: Sketch of final experiment setup.

APPENDIX A. FIRST APPENDIX

Table A.0.1: Measurements for test- and final experimental setup.

Symbol	Test-setup measurement [mm]	Final-setup measurement [mm]
D	360	500
L	180	250
H_T	400	400
H_C	1150	1400
h_T	380	200
h_R	270	150
h_d	35	35
t_T	5	5
t_d	3	3
t_L	56	56

Items needed for a final larger scale experimental setup:

- Light source: 3×4 pc Aputure AL-H160 LED-panels.
- Diffusor: 1 pc 500×500 mm frosted acrylic plate with a thickness of 3 mm.
- Water tank: 1 pc glass tank with measurements $500 \times 200 \times 5$ mm (diameter, height, thickness).

Using LED-panels instead of sodium light makes it possible to tweak the intensity of the light. Moreover, sodium lamps have a 5–10 minutes warm-up time to illuminate with full intensity; LED lamps illuminate with full intensity without any warm-up time. In setup 4.1.2b, one LED-panel illuminates a circle with a diameter of approximately 22 cm. The LED has the measurements $15.1 \times 5.6 \times 10$ cm. To illuminate a circle with a diameter of 50 cm there needs to be 3×4 pc LED-panels placed side by side.

Using the frosted acrylic plate as a diffusor instead of, for instance, an A4 drafting paper or a cloth, gives more homogenous illumination without adding background noise in the form of paper fibers or wrinkles.

APPENDIX A. FIRST APPENDIX



The image shows the front page of a datasheet for the MotionBLITZ EoSens® mini1 camera. At the top left is a photograph of an owl's face. To the right of the owl is the text "High-Speed Recording Cameras". Below the owl is the product name "MotionBLITZ EoSens® mini1" and the subtitle "High-Speed Recording Camera".

Innovative Technology for Maximum Light Efficiency

Lighting Becomes a Minor Matter
So far, lighting was the crucial point in high-speed recording. The MotionBLITZ EoSens® mini1 resolves the lighting issue! Its unprecedented sensitivity enables real high-speed recordings under normal lighting conditions.

Crystal Clear Images
Every single pixel is adjusted regarding blackvalue and dynamic, in real time. The benefits are low noise and crystal clear pictures.

Onboard Ring Buffer (Pre-/Post-Trigger)
The onboard Ring Buffer allows buffering of triggered events up to 6.6 seconds at full resolution and full speed. Freely adjustable pre or post triggered recording time to capture the event as it happens.

ImageBLITZ® Automatic Trigger
The ImageBLITZ® Automatic Trigger allows object-driven triggering directly through the camera by a user defined image region. Adjusting this image area acts as a trigger sensor. If there is a change in the lightness (on the single frame level), the camera will trigger automatically.

MotionBLITZ EoSens® mini1 Advantages at a Glance:

- Maximum photo sensitivity: 2,500 ASA monochrome, 2,000 ASA RGB
- Up to 508 frames per second at 1,280 x 1,024 pixel resolution
- Stepless adjustable frame rate up to more than 100,000 frames per second at reduced resolution
- Up to 6.6 seconds onboard Recording Memory at full resolution and full speed
- GigE Vision® compatible
- ImageBLITZ® Automatic Trigger
- Crashproof up to 100 g shock, 10 g vibration
- High image quality through pixel based FPN-Correction
- Burst Trigger Mode
- Multi Sequence Mode



Figure A.0.2: Camera datasheet.

APPENDIX A. FIRST APPENDIX

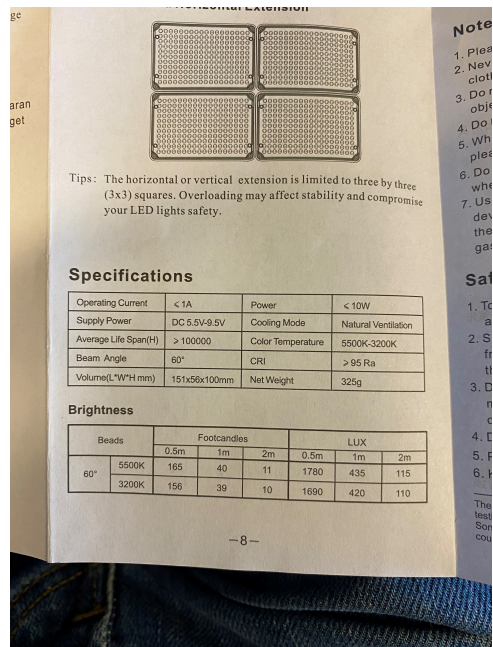


Figure A.0.3: LED-panel datasheet.